Development of green engineered cementitious composites with acceptable dynamic split resistance utilising recycled polymer fibres

Meng Chen [a], Run Jiang [a], Tong Zhang [a,*], Hui Zhong [b], Mingzhong Zhang [b]

[a] School of Resources and Civil Engineering, Northeastern University, Shenyang 110819, China

[b] Department of Civil, Environmental and Geomatic Engineering, University College London, London, WC1E 6BT, UK

Abstract

Using recycled tyre polymer fibres (RTPF) to replace part of polyvinyl alcohol fibres (PVAF) is a strategy to produce green and economical engineered cementitious composites (ECC). This paper systematically investigated the influence of RTPF dosage (0.25–1.0 vol%) on split tensile performance of ECC under different strain rates. Results indicated that replacing PVAF with RTPF up to 0.5 vol% could still show a pronounced strain-hardening behaviour for ECC, although accompanied by a decrease in static split tensile strength. The dynamic split tensile performance of all ECC mixes was strongly sensitive to strain rate and all hybrid fibre reinforced ECC presented a greater strain rate effect than the mono-PVAF reinforced ECC. Under dynamic split tension, the specimens with various RTPF dosages could maintain their structural integrity. This paper suggested that RTPF can be adopted to replace part of PVAF to produce a greener and more economical ECC with satisfactory static and dynamic mechanical performance but the highest substitution amount should be set to 0.5 vol%.

Keywords: Strain hardening behaviour; Recycled polymer fibre; SHPB test; Dynamic increase factor; Strain rate effect

1. Introduction

Engineered cementitious composites (ECC) have attracted increasing attention recently owing to their unique features as compared with conventional concrete, which can exhibit superior ductility along with strain-hardening and multiple cracking behaviour [1-3]. These special properties can be bestowed and modified by using the micromechanical theory that considers the interactions between fibre, matrix and their interface [1, 4]. Up to now, most of the developed ECC mixtures utilise polyvinyl alcohol (PVA) or polyethylene (PE) fibres as the main constituents, and these fibres are more expensive than other commercially available fibres [5-9]. According to previous studies,

approximately 50–90% of all expenses for producing the ECC are from PVA or PE fibres [10, 11]. Therefore, it is highly essential to seek other low-cost and sustainable fibres for ECC.

Polypropylene (PP) fibres have been used to replace PVA fibres in ECC as they are cheaper and less energy-intensive than PVA fibres [11-13]. For instance, an ECC mixture with an excellent tensile strain capability of 6–9% was successfully developed using low-carbon cement and PP fibres [14]. Besides, it was reported that the material cost, embodied carbon and embodied energy of such PP fibre reinforced ECC made with limestone calcined clay cement were 61%, 48% and 45% lower as compared with a typical PVA reinforced ECC [15]. The feasibility of using PP fibres in ECC has also been assessed in other studies [16-18]. However, the production of virgin synthetic fibres can result in inevitable environmental impacts [19], hindering sustainable development if PP fibres are used in large quantities to manufacture ECC. To improve the sustainability of ECC, one of the emerging solutions is to use recycled fibres in ECC [19-21]. To date, only a few studies have focused on the feasibility of using recycled fibres to produce ECC [20, 22, 23]. It was found that recycled polyethylene terephthalate (PET) fibres obtained from plastic bottles were feasible to partially replace the PVA fibres in ECC to maintain acceptable strain-hardening and multiple cracking performances [20, 23]. The material cost and environmental impact of the developed hybrid PET and PVA fibre reinforced ECC were considerably lower than those of ECC with PVA fibres only. Hybridising 1.0 vol% recycled PET fibre and 1.0 vol% PVA fibre in ECC can achieve similar impact behaviour compared to ECC with 2.0 vol% PVA fibre [23].

Apart from the aforementioned recycled fibre, another type of recycled polymer fibre attained from end-of-life tyres has been increasingly investigated lately [24-26]. The main focus of the ongoing research work is to explore the feasibility of incorporating this recycled tyre polymer (RTP) fibre into cementitious materials as the successful utilisation can not only promote sustainable development but can also mitigate the environmental problems caused by the large amounts of end-of-life tyres [27-29]. The existing studies revealed that RTP fibres were feasible to replace virgin PP fibres in concrete mainly considering the shrinkage behaviour, flexural fatigue performance, dynamic mechanical properties and behaviour at elevated temperatures [28, 30-33]. Given the benefits of using RTP fibres in cementitious materials, it is promising to replace PVA fibres in ECC with these sustainable and low-cost fibres. However, the relevant study in this field is very limited.

Zhong et al. [22] studied the feasibility of using RTP fibre to develop ECC and evaluated the influence of RTP fibre content on the static and dynamic compressive properties of ECC. They found that ECC containing RTP fibre of up to 0.5 vol% can still show acceptable tensile strain capacity, and ECC with hybrid PVA and RTP fibre had a stronger strain rate effect than ECC with mono-PVA fibre. It is worth noting that ECC may experience split tensile failure more easily under extreme loading conditions. Therefore, it is important to understand the static and dynamic split tensile behaviour of hybrid RTP fibre and PVA fibre reinforced ECC, which have not been comprehensively assessed yet.

The main purpose of this study is to study the influence of the replacement content of RTP fibres to PVA fibres (0.25, 0.5, 0.75 and 1.0 vol%) on the dynamic split tensile properties of ECC through a series of experiments. The mixture with 2.0 vol% PVA fibre was prepared as a reference. Firstly, the static split tensile strength of all mixtures was measured, which is an important parameter to analyse the dynamic tensile behaviour. Then, the split tensile properties under different strain rates (4.23–10.95 s^{-1}), including failure mode, stress-time response, dynamic increase factor (DIF) and energy dissipation, were measured using a split Hopkinson pressure bar (SHPB) with a diameter of 100 mm. Based on the experimental results and by considering the fibre physical parameters (content and aspect ratio), empirical models were proposed to describe the relationship between DIF and strain rate. The fibre bridging mechanism of proposed ECC mixes under dynamic loadings was explored using a portable microscope and scanning electron microscopy (SEM) technique.

2. Experimental programme

2.1 Materials

Ordinary Portland cement (P.I. 42.5) with a specific gravity of 3.09 and low calcium fly ash with a specific gravity of 2.19 were used as binder materials. Fine silica sand with a specific gravity of 2.66, a maximum particle size of 250 μm and an average particle size of 130 μm was used as fine aggregate. The particle size distribution of these materials is shown in Table 1. To enhance the flowability of specimens, polycarboxylate-based superplasticizers were added to all mixtures. The RTP fibres used in this study were the same as those used in previous studies [22, 26]. A screening method reported in a previous study [33] was used to remove the rubber particles and some impurities from RTP fibres. The physical appearance of PVA and RTP fibres is shown in Fig. 1. It

should be noted that the dimension and main properties of RTP fibres mentioned below were characterised by a previous study [26]. The PVA fibres have a length of 12 mm, a diameter of 40 μm and a density of 1300 kg/m^3. The length of RTP fibres is only 5.2 ± 2.4 mm with a diameter of 21.4 ± 4.4 μm and a density of 1476 ± 3.0 kg/m^3. The length and diameter distribution of RTP fibres are presented in Table 2 and Table 3, respectively. About 80.34% of RTP fibres are between 2–8 mm in length and 82.66% are between 10–26 μm in diameter. The tensile strengths of PVA fibres and RTP fibres are 1560 MPa and 761 ± 115 MPa, respectively. The elastic modulus of PVA fibres and RTP fibres are 41 GPa and 3.8 ± 0.7 GPa, respectively.

Table 1 Particle size distribution of cement, fly ash and silica sand.

Matrix ingredient	D_{10} (μm)	D_{50} (μm)	D_{90} (μm)
Cement	1.43	10.49	28.90
Fly ash	2.78	12.53	42.33
Sand	103.63	145.71	213.15

Note: D10, D50 and D90 = Particle size with cumulative distribution of 10%, 50% and 90% [34].

Table 2 Length distribution of RTP fibres.

Length (mm)	0-2	2-4	4-6	6-8	8-10	10-13
Frequency (%)	6.33	27.67	30.67	22	9.33	4

Table 3 Diameter distribution of RTP fibres.

Diameter (μm)	10-14	14-18	18-22	22-26	26-30	30-32
Frequency (%)	7.33	12	37.33	26	15.33	2

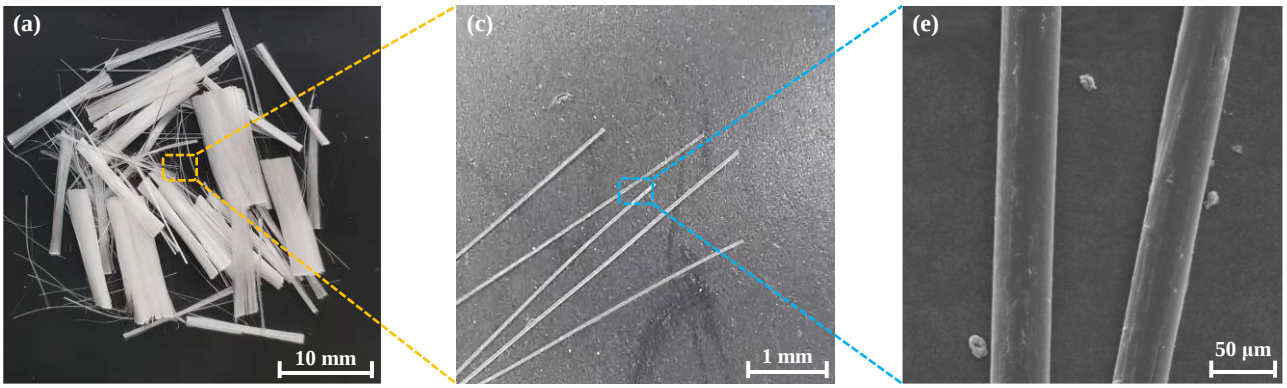

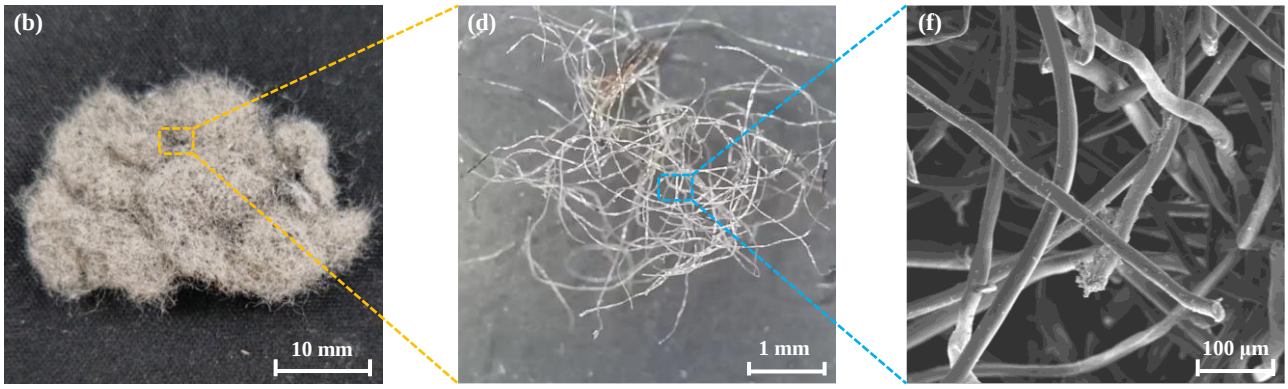

Fig. 1. Physical appearance of PVA and RTP fibres.

2.2 Mix proportions and sample preparation

Table 4 lists the mix proportions of ECC used in this study, which was the same as the one in a previous study [22]. The meaning of V1.5T0.5 represents the cementitious matrix reinforced with two types of fibres, where 'V1.5' represents the amount of PVA fibre (1.5% by volume) while 'T0.5' stands for the amounts of RTP fibre (0.5% by volume). It is worth noting that V2.0 was the control group without any RTP fibres. The other four mix proportions were compared with it to explore the effect of RTP fibre replacement on the dynamic split tensile properties of ECC. To ensure that the proposed ECC mixtures can exhibit obvious strain-hardening behaviour and acceptable mechanical properties, the maximum RTP fibre substitution amount was set to 1 vol% [22].

Table 4 Mix proportions.

Mixture ID	Weight ratio					Volume (%)	
	Binder		Silica sand/ binder	Water/ binder	Superplasticiser/ binder	PVA fibre	RTP fibre
	Cement	Fly ash					
V2.0	0.45	0.55	0.36	0.27	0.004	2.0	0
V1.75T0.25						1.75	0.25
V1.5T0.5						1.5	0.5
V1.25T0.75						1.25	0.75
V1.0T1.0						1.0	1.0

2.3 Sample preparation

The sample preparation process is shown in Fig. 2. It should be noted that RTP fibres were first mixed with part of all mixing water to ensure better dispersion of the fibres [32, 35, 36]. When the fibres were evenly distributed in the mixture, the mixing stopped. The total mixing time was about

15 minutes. All de-moulded samples were placed in the standard curing room (20 ± 2 ℃ and 95% RH) until 28 d.

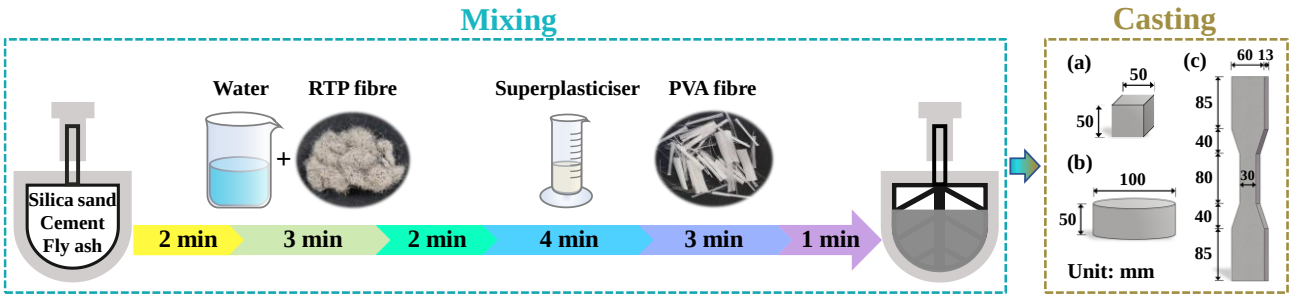

Fig. 2. Preparation process of proposed ECC specimens.

2.4 Test methods

2.4.1 Static split tensile test

Brazilian disk specimens were fabricated to determine the static splitting tensile strength of ECC. For the static splitting tensile test, the results are valid only when the first crack occurs around the central region of the specimen [37, 38]. To ensure the results are valid, the Brazilian disc sample with a dimension of Ø 100 mm × 50 mm was manufactured for the static splitting tensile test [32, 39-41], which was similar to that used for the dynamic split tensile test. The following equation was adopted to calculate the static splitting tensile strength of all ECC mixes [42, 43].

$$f_{st} = \frac{2F_p}{\pi DL} \tag{1}$$

where f_{st} is the static splitting tensile strength of the specimen, F_p is the maximum load during the static splitting tensile test, D is the diameter of the sample, and L is the height of the specimen.

2.4.2 Dynamic splitting tensile test

The splitting tensile behaviour of the specimens at different strain rates (10^{-1} to 10^{1} s^{-1}) was measured using a 100 mm diameter SHPB test device, the schematic diagram of which is presented in Fig. 3. The main components of the SHPB testing device included a striker bar, an incident bar, a transmitted bar and an absorbing bar made of high-quality alloy steel, with lengths of 600 mm, 5000 mm, 3500 mm and 1200 mm, respectively.

Prior to the test, the Brazilian disc specimen was placed between the incident and transmission bars, as shown in Fig. 3. During the test, the incident bar was first impacted by the striker bar which generates an incident wave ($\varepsilon_i(t)$). During the propagation of the incident wave, part of the incident wave was reflected as a reflected wave ($\varepsilon_r(t)$) when it reached the interface between the bar and the

specimen. The rest passed via the transmission bar as the transmitted wave ($\varepsilon_t(t)$) [44]. A rubber pulse shaper with a diameter of 60 mm and a thickness of 2 mm was used to help achieve the dynamic stress equilibrium during the SHPB test [28, 45]. An example of how to check the stress equilibrium state is shown in Fig. 4, suggesting the achievement of the dynamic stress equilibrium for the test specimen as its transmitted stress was very close to the sum of the incident stress and the reflected stress. The strain gauge mounted on the incident bar was used to record the incident and reflected strains, while the strain gauge on the transmission bar was applied to measure the transmitted strain [28]. The change of force with time ($F_d(t)$) acting on the specimen can be calculated as follows [38]:

$$F_d(t) = E_0 A \varepsilon_t(t) \tag{2}$$

where A and E_0 represent the cross-sectional area and elastic modulus of the bar, respectively.

The change in stress over time ($f_{dst}(t)$) can be evaluated using Eq. (1) by inputting the change in force obtained from Eq. (2). The loading rate and strain rate corresponding to each specimen can be calculated as:

$$\dot{\sigma} = \frac{f_{dst}}{\Delta t} \tag{3}$$

$$\dot{\varepsilon} = \frac{\dot{\sigma}}{E_s} \tag{4}$$

where f_{dst} denotes the peak stress of the stress-time curve of the sample, Δt is the time when the specimen reaches f_{dst}, and E_s is the elastic modulus of the specimen.

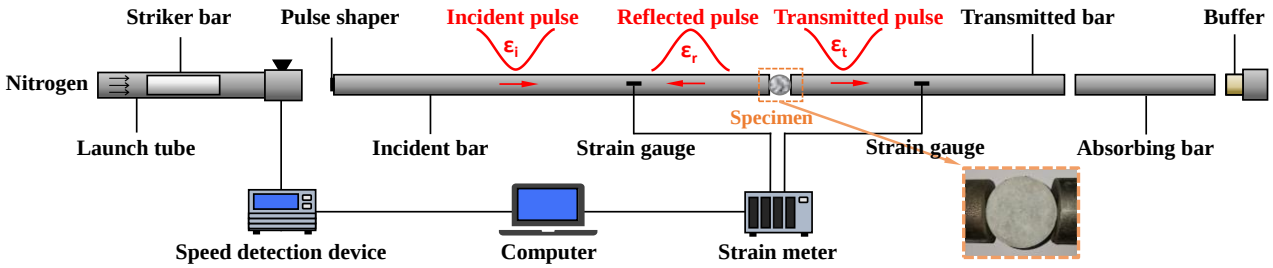

Fig. 3. Schematic diagram of SHPB testing system.

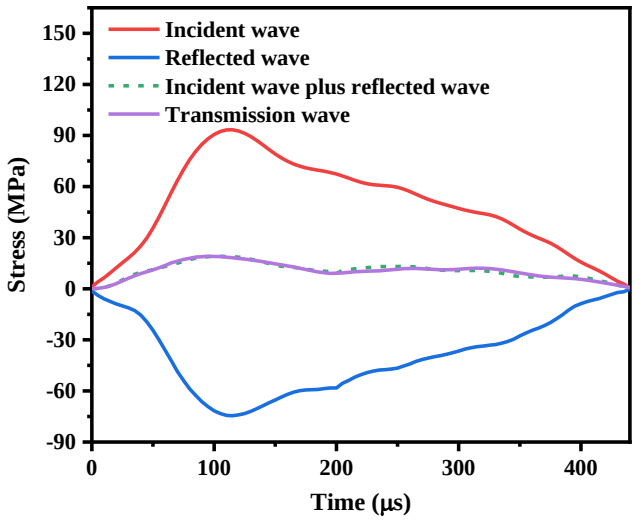

Fig. 4. An example of checking the stress equilibrium.

2.4.3 Morphology observation of fibres

To explore the morphology of PVA and RTP fibres after the SHPB tests, some fracture pieces of ECC samples were carefully extracted and collected for SEM analysis. Additionally, a portable microscope was used to analyse the fibre bridging mechanism at the crack interfaces of specimens.

3. Results and discussion

3.1 Static splitting tensile strength

Fig. 5 depicts the uniaxial tensile stress-strain curve of each mixture. All mixtures exhibited strain-hardening behaviour under uniaxial tensile loading. Compared with V2.0, the strain-hardening stage of the mixture decreased with the increase of RTP fibre content, as well as the first cracking strength and tensile strength, pointing out that the incorporation of RTP fibres was not beneficial to the uniaxial tensile behaviour of ECC [22]. However, when the RTP fibre content was equal to or less than 0.5 vol%, the mixtures still possessed a tensile strain capacity of greater than 2%. A similar finding was reported in a previous study [26] that replacing PVA fibres with RTP fibres did not improve the uniaxial tensile behaviour of fly ash-slag based fibre reinforced geopolymer composites. After de-bonding from the matrix, PVA fibres can either experience increasing or constant frictional bonding stress as they are pulling out from the matrix. While RTP fibres would mostly experience constant bonding stress due to their hydrophobic surface feature. This can be evidenced by the levelling out of the uniaxial tensile stress-strain curve of ECC containing both PVA and RTP fibres [46].

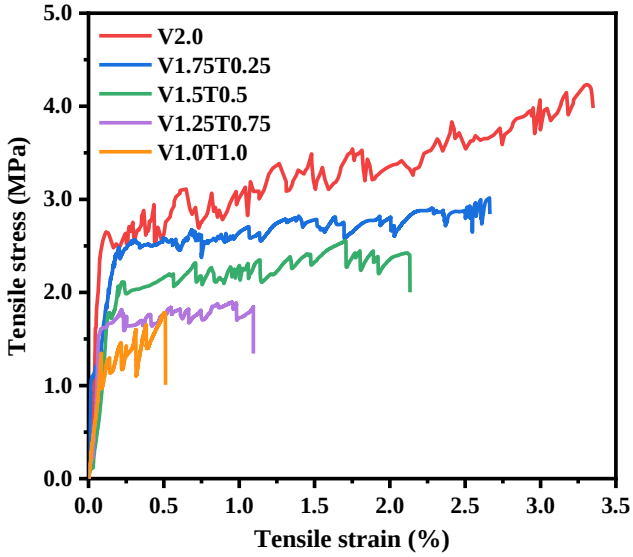

Fig. 5. Tensile stress-strain curves of all mixtures [22].

The static splitting tensile strength of all mixtures is shown in Fig. 6. The static splitting tensile strength of ECC decreased with the replacement of PVA fibres by RTP fibres, which is similar to the trend of uniaxial tensile strength [22]. The static splitting tensile strength of V2.0 was 0.9%–70.7% higher than that of hybrid fibre reinforced ECC, suggesting that RTP fibres in improving the static tensile strength of ECC were poorer than PVA fibres, primarily because of the physical properties of RTP fibres (e.g., smaller dimension as compared with PVA fibres) [40]. Besides, the poor bonding between the RTP fibre and the matrix can also contribute to the reduction of the static tensile strength of ECC [22]. However, replacing 0.25% PVA fibre with RTP fibre did not significantly weaken the static splitting tensile strength of ECC, which can be attributed to the synergistic hybrid fibre effect in restraining the cracks, where RTP fibres were effective in controlling the micro-cracks while PVA fibres tended to arrest some larger cracks.

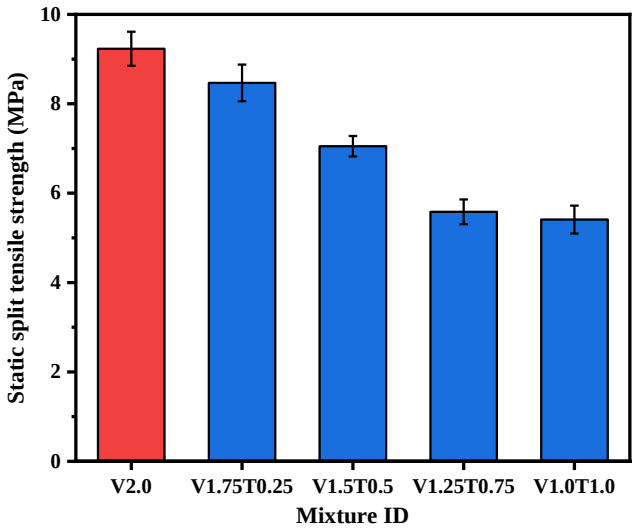

Fig. 6. Static splitting tensile strength of all mixtures.

3.2 Dynamic splitting tensile behaviour

3.2.1 Failure pattern

The failure patterns of all mixtures under static and dynamic loadings are shown in Fig. 7. The major cracks of all mixes were generated at the central region and were then propagated along the loading direction until the complete failure [47]. All ECC samples exhibited similar failure modes under static loadings, with one small splitting crack along the loading direction. It implies that the integrity of the test sample can be maintained when 0.25-1.0% PVA fibre was replaced with RTP fibre. Under dynamic splitting tension, the damage degree of the specimen was increased with the increasing strain rate, especially in terms of the crack width and length. Apart from the major split crack, some additional fine cracks were developed in some mixes. For instance, an unconnected fine crack was observed near the main crack for V1.75T0.25 when the strain rate was between 8.28 s^{-1} and 8.62 s^{-1}. When the strain rate exceeded around 8.28 s^{-1}, the two loading end faces of the specimen experienced a triangular local compression failure, where this phenomenon was more pronounced at a higher strain rate. Many previous studies have captured this type of failure under dynamic split tensile loadings [40, 48, 49], which could be attributed to that the stresses at the loading faces are larger than the compressive strength of the test sample before the crack penetration in the central region [50]. When the strain rate was within 10.68 s^{-1} and 10.95 s^{-1}, the triangular failure of V1.0T1.0 was the most severe among all ECC mixes, which could be due to its poorest static compressive strength [22]. Considering the failure modes, replacing PVA fibres with RTP fibres up to 1.0 vol.% can still achieve an acceptable resistance to dynamic split tension for ECC.

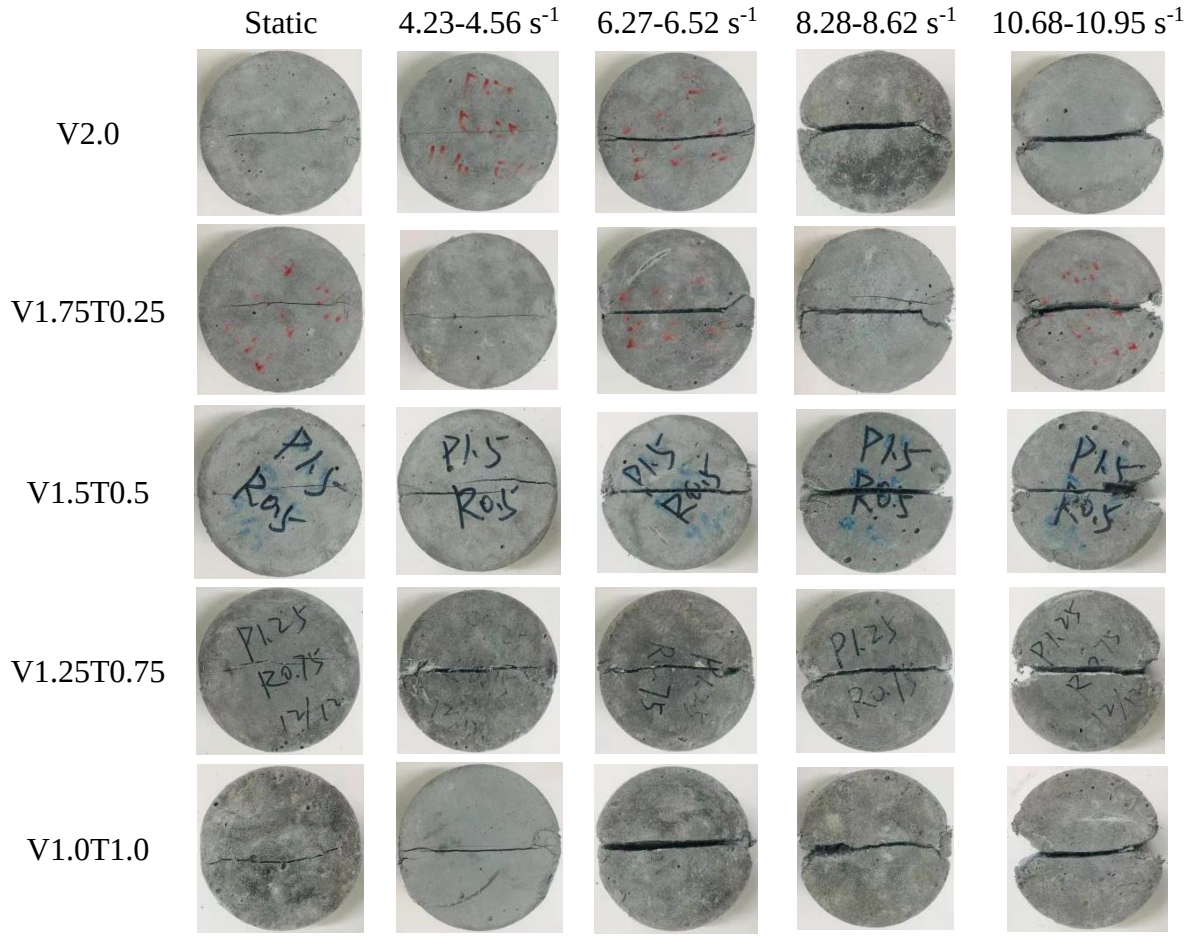

Fig. 7. Failure patterns of all mixtures under different strain rates.

3.2.2 Stress-time curves

Fig. 8 depicts the stress-time curves of all mixtures at strain rates ranging from 4.23 s^{-1} to 10.95 s^{-1}. The curve shape of all ECC specimens was similar, consisting of three parts including the ascending, descending and fluctuation stages [39]. When the ECC test sample was impacted by the incident bar, it would first undergo elastic deformation followed by a non-linear deformation before reaching the peak stress. The first visible crack appeared during the non-linear deformation stage and the fibres started restraining the induced crack. After exceeding the peak stress, the induced crack quickly propagated along with fibres pulling out or rupturing. Previous studies have observed similar fluctuation parts during the dynamic split tension [39, 51, 52]. This phenomenon could be ascribed to the increasing contact area between the test specimen and the bars [51] or the progressive pull-out of fibres as the growth of cracks [39]. As seen in Fig. 8, the fluctuation part was less pronounced when more PVA fibres were replaced with RTP fibres, due to the poorer interfacial bonding strength of RTP fibres as compared to PVA fibres. As mentioned in Section 3.1, some PVA fibres may experience rising frictional bonding stress as they are pulling out from the matrix, which can

considerably improve the bonding behaviour of the whole composite. As reported in the previous research [39], the overall curve shape of ECC became smooth when it was heated at a temperature of over 250 °C because of the reduced fibre bridging caused by the melting of PVA fibres.

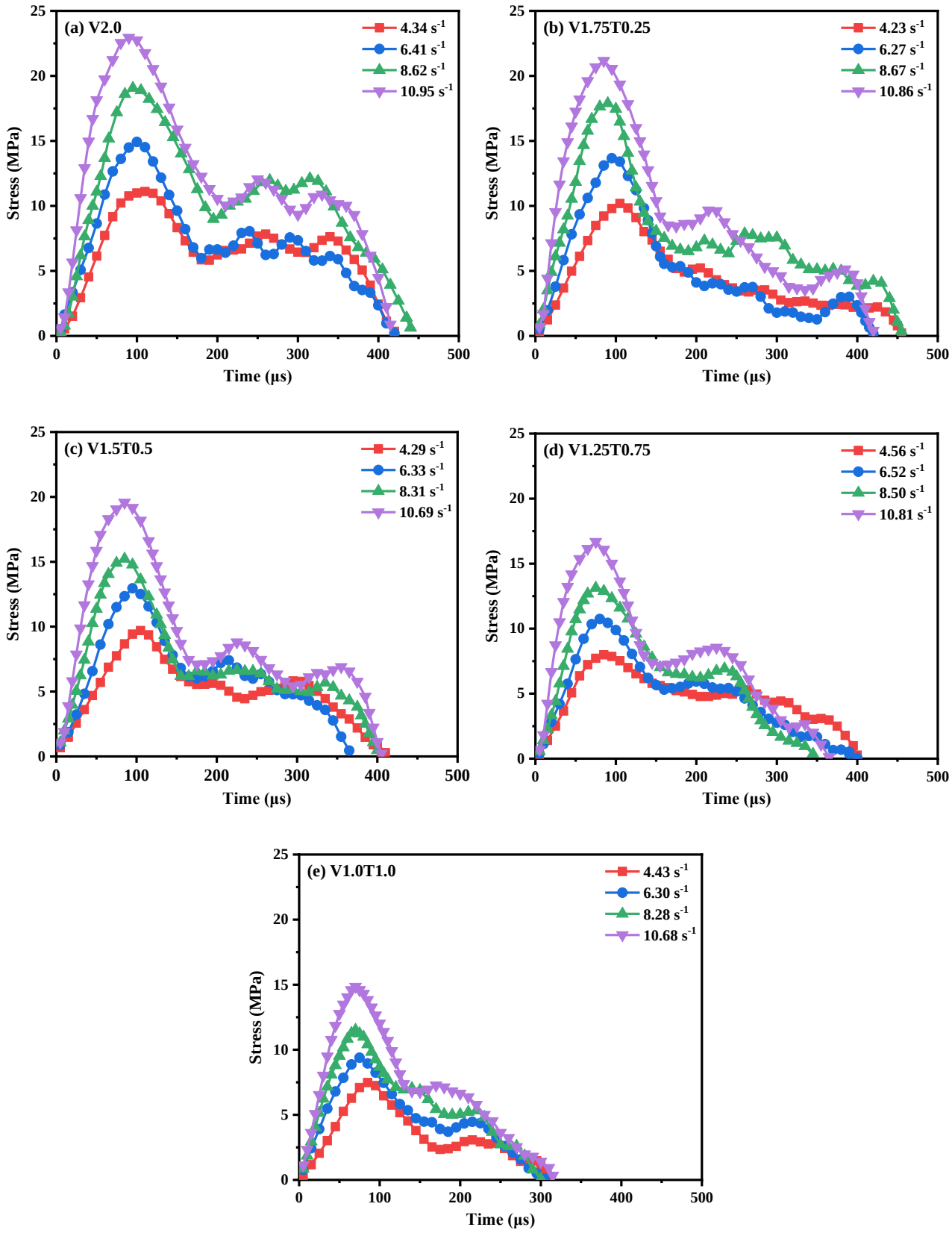

Fig. 8. Effect of strain rate on stress-time curves of (a) V2.0, (b) V1.75T0.25, (c) V1.5T0.5, (d) V1.25T0.75, and (e) V1.0T1.0.

3.2.3 Dynamic splitting tensile strength

Fig. 9 demonstrates the effect of strain rate on the dynamic splitting tensile strength (i.e., peak stress in the stress-time response) of ECC. Similar to the dynamic compressive strength of ECC [22], the dynamic split tensile strength of all investigated mixes herein was enhanced with the increasing strain rate. For instance, the dynamic split tensile strength of V2.0 was increased from 11.1 MPa to 22.94 MPa when the strain rate was changed from 4.34 s^{-1} to 10.95 s^{-1}. Additionally, the dynamic split tensile strengths of V1.5T0.5 and V1.0T1.0 were increased by 101.8% and 98.5%, respectively, when the strain rate was increased from 4.29 s^{-1} to 10.69 s^{-1}. The increment of dynamic split tensile strength with strain rate can be mainly ascribed to the structural effects (e.g., lateral inertial effect), rapid formation and propagation of cracks and Stefan effect [40, 53]

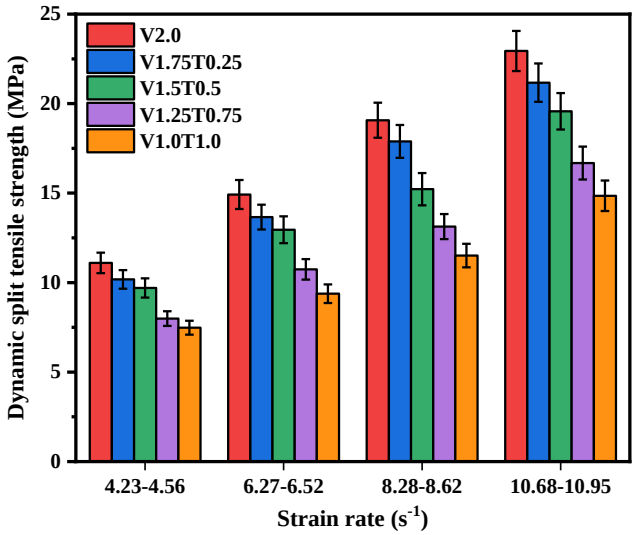

Fig. 9. Effect of strain rate on dynamic split tensile strength of all mixtures.

The dynamic splitting tensile strength of V2.0 was higher than that of all hybrid fibre reinforced ECC mixtures when the strain rate was similar, which is consistent with the trend of static split tensile strength. For instance, when the strain rate was between 8.28 s^{-1} and 8.62 s^{-1}, the dynamic split tensile strength of hybrid fibre reinforced ECC was 6.2%–39.6% smaller than that of V2.0. The higher dynamic split tensile strength observed in ECC with more PVA fibres can be mainly ascribed to the stronger fibre bridging action provided by PVA fibres under dynamic split tension. Due to the strain rate effect, the improvements in the properties of PVA fibres were larger than those of RTP fibres, making PVA fibres better control the induced split cracks and thereby

higher ultimate strengths for the whole composites [22].

3.2.4 Dynamic increase factor

The effect of RTP fibre content on the DIF of ECC under different strain rates is shown in Fig. 10. For each mix, the trend of DIF with strain rate was similar to that of dynamic split tensile strength, where the DIF of ECC was increased with the rise of strain rate. While the tendency of DIF with fibre content was opposite to that of dynamic split tensile strength, suggesting that the hybrid fibre reinforced ECC had a greater strain rate sensitivity than mono-PVA fibre reinforced ECC. For instance, the DIF of V2.0 ranged from 1.2 to 2.49 while that of V1.25T0.75 was in the range of 1.43 and 2.99. This shows a good agreement with the DIF of ECC under dynamic compression [22], which could be associated with the stronger Stefan effect and lower internal quality of specimens containing RTP fibres [54, 55]. Fig. 11 depicts the fitted linear curve between DIF and strain rate for each ECC mixture, and the fitted equations are summarised in Table 4. According to derived R^2 values, all proposed DIF equations had high reliability in predicting the material behaviour under high strain rates.

Table 4 Summary of the fitted DIF equations for the logarithm curves.

Mixture ID	Fitted equation of DIF	R^2
V2.0	DIF=3.195 log$\dot{\varepsilon}$ - 0.886	0.981
V1.75T0.25	DIF=3.174 log$\dot{\varepsilon}$ - 0.841	0.980
V1.5T0.5	DIF=3.399 log$\dot{\varepsilon}$ - 0.834	0.945
V1.25T0.75	DIF=4.071 log$\dot{\varepsilon}$ - 1.325	0.962
V1.0T1.0	DIF=3.486 log$\dot{\varepsilon}$ - 0.960	0.938

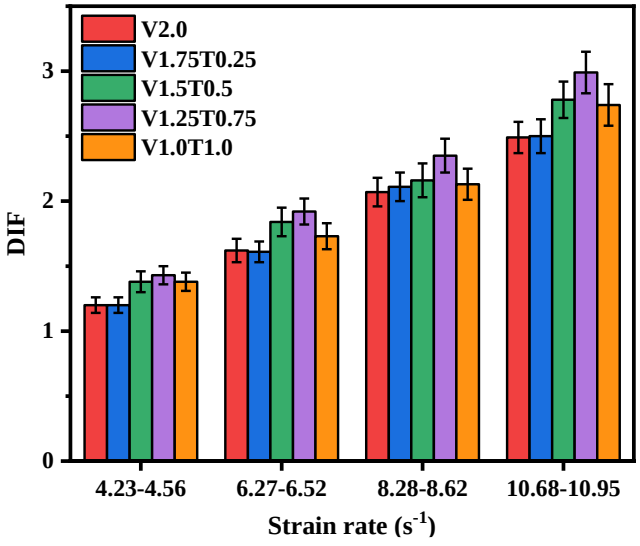

Fig. 10. Effect of strain rate on DIF of all mixtures.

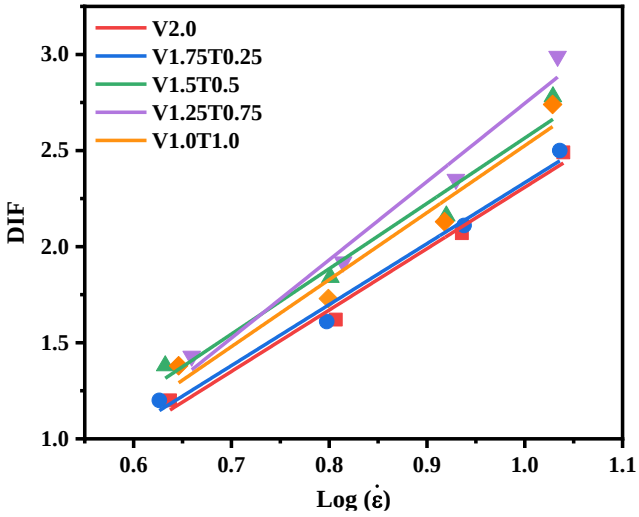

Fig. 11. Fitted curves of DIF.

The bilinear model was a commonly used model to describe the relationship between DIF of split strength and logarithmic strain rate as shown in Eq. (5) [48, 56].

$$DIF = \begin{cases} a\,\dot{log}\,\varepsilon + b, \dot{\varepsilon} \le \dot{\varepsilon}_i \\ c\,\dot{log}\,\varepsilon + d, \dot{\varepsilon} > \dot{\varepsilon}_i \end{cases} \tag{5}$$

where $\dot{\varepsilon}$ is the strain rate obtained from the experiment and $\dot{\varepsilon}_i$ is the critical strain rate for the bilinear model, a and b are the featured parameters within the static strain rate range, c and d are the featured parameters of the second line within the dynamic strain rate range.

However, the equation obtained by the simple fitting method cannot reflect the influence of fibre physical size and hybrid fibre interaction on the DIF of ECC. Hence, the bilinear interpolation algorithm was used to determine the featured parameters of the second line in the bilinear model [57], and further established the correlation between the volume fraction and aspect ratio of hybrid fibres and DIF as follows:

$$c = c_1 v_V \lambda_V + c_2 v_T \lambda_T + c_3 v_V \lambda_V v_T \lambda_T + c_4 \tag{6}$$

$$d = d_1 v_V \lambda_V + d_2 v_T \lambda_T + d_3 v_V \lambda_V v_T \lambda_T + d_4 \tag{7}$$

where v_V and λ_V are the volume fraction and aspect ratio of PVA fibres, v_T and λ_T are the volume fraction and aspect ratio of RTP fibres, and the other symbols denote the fitted parameters.

The featured parameters of the improved DIF bilinear model were determined by the following steps: (i) Based on the experimental results, performing the simple linear fitting approach on the DIF and logarithmic strain rate of each mixture to obtain the initial values of the second line (c and d), (ii) Re-fitting the initial featured parameters c and d by using Eq. (6) and Eq. (7) to attain the fitted

parameters for the two equations, as listed in Table 5, (iii) Recalculating the featured parameters c and d through Eq. (6) and Eq. (7) to obtain the equation of the second line in Eq. (5), as listed in Table 6, (iv) Connecting the static value obtained from the experiment (i.e., DIF = 1.0) with the starting point of the second line to determine the equation of the first line in Eq. (8). Based on the results of pre-experiments, the failure mode of the specimen under the strain rate of about 4.42 s^{-1} was similar to that under static split tension, so 4.42 s^{-1} was considered as the critical strain rate [58].

Fig. 12 compares the prediction results of the improved bilinear model with the experimental DIF values of all mixes. To verify the reliability of the model fitting method, the R^2 between the predicted logarithm curve and the experimental test data were calculated. The results showed that all R^2 of the first line of the improved bilinear models were higher than 0.912, while an even higher R^2 of more than 0.927 appeared for the second line of the models. Thus, the predicted results show a good agreement with the experimental results, considering the fibre type and content.

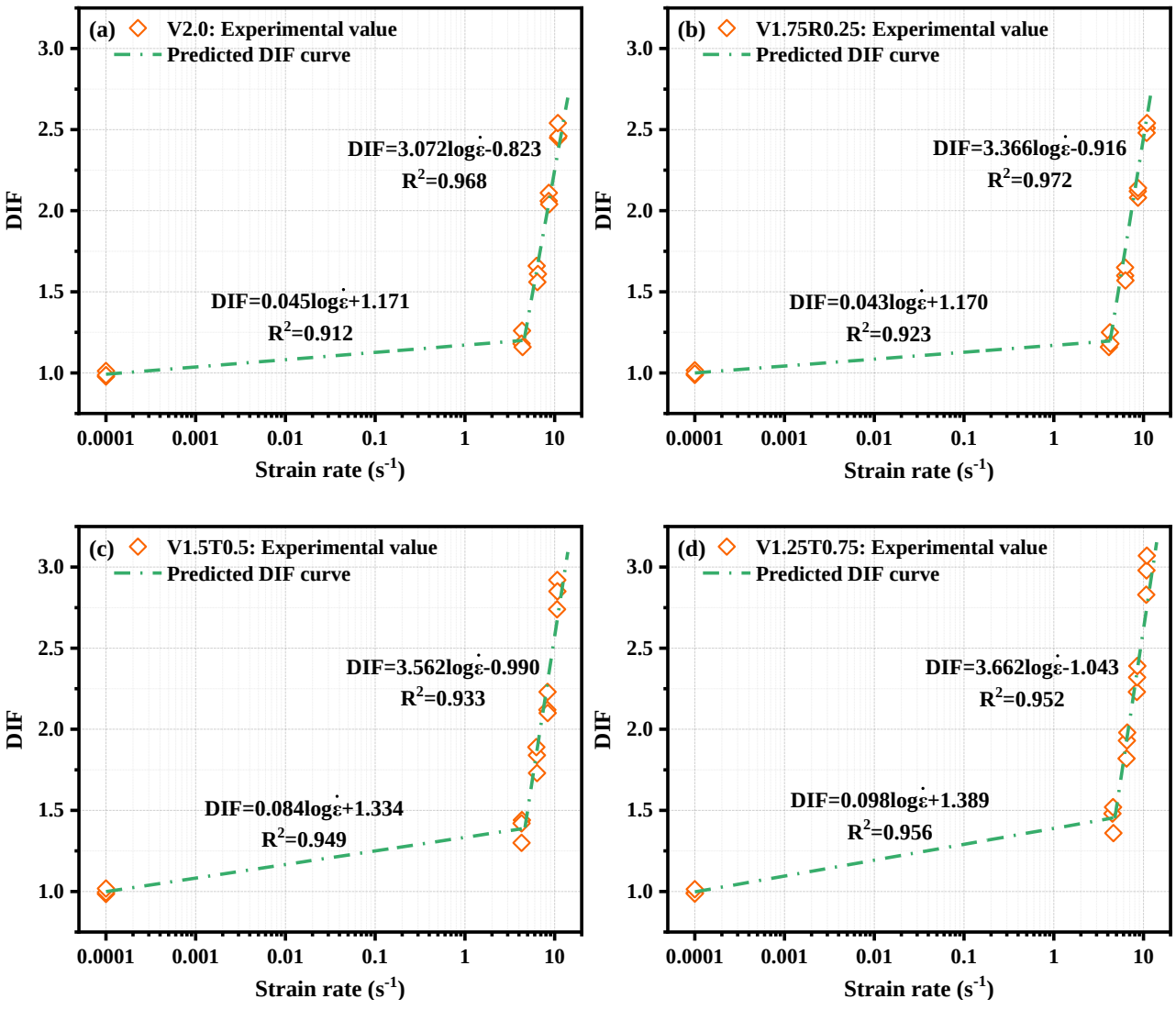

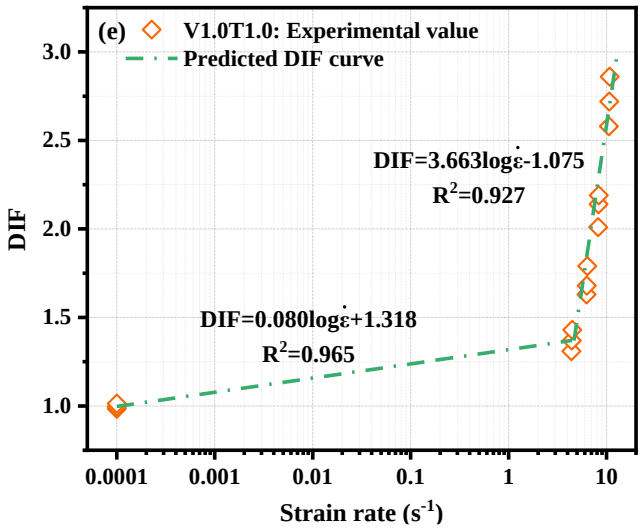

Fig. 12. Comparison of predicted curves and experimental results between DIF and logarithmic strain rate of ECC mixtures: (a) V2.0, (b) V1.75T0.25, (c) V1.5T0.5, (d) V1.25T0.75, (e) V1.0T1.0.

Table 5 Fitted values of the Eq. (6) and Eq. (7).

c_1	c_2	c_3	c_4	d_1	d_2	d_3	d_4
0.605	0.670	0.107	-0.558	0.219	0.233	-0.022	-2.134

Table 6 Coefficients of the fitted DIF equation.

Coefficient	V2.0	V1.75T0.25	V1.5T0.5	V1.25T0.75	V1.0T1.0
a	0.045	0.043	0.084	0.098	0.080
b	1.171	1.170	1.334	1.389	1.318
c	3.072	3.366	3.562	3.662	3.663
d	-0.823	-0.916	-0.990	-1.043	-1.075

3.2.5 Energy dissipation capacity

During the SHPB test, the dissipated energy ($W_d(t)$) of all mixtures can be calculated based on the energy balance between incident energy ($W_i(t)$), reflected energy ($W_r(t)$) and transmitted wave ($W_t(t)$), using the following equations [37]:

$$W_d(t) = W_i(t) - W_r(t) - W_t(t) \tag{8}$$

$$W_i(t) = E_0 C_0 A \int_0^t \varepsilon_i^2(t)dt \tag{9}$$

$$W_r(t) = E_0 C_0 A \int_0^t \varepsilon_r^2(t)dt \tag{10}$$

$$W_t(t) = E_0 C_0 A \int_0^t \varepsilon_t^2(t)dt \tag{11}$$

where C_0 stands for the longitudinal wave velocity of the SHPB bar.

The dissipated energy of all mixtures is demonstrated in Fig. 13. The energy dissipation of all ECC mixes was increased with the increase of strain rate, which is consistent with the trends of dynamic split tensile strength and DIF. For instance, the dissipated energy of V2.0 and V1.0T1.0 were increased by 133.7% and 210.3%, respectively, when the strain rate was increased from 4.34 s^{-1} to 10.95 s^{-1}. The increase in energy dissipation of ECC under a high strain rate can be mainly attributed to the rapid appearance of micro-cracks and fast propagation of main splitting cracks [41, 59].

Replacing PVA fibres with RTP fibres significantly reduced the energy dissipation of ECC. Within the considered strain rate range, the dissipated energy of V1.5T0.5 and V1.0T1.0 was 13.3%–21.5% and 29.5%–47.7% lower than that of V2.0, respectively. Figs. 14 and 15 illustrate the fibre conditions of PVA and RTP fibres after the dynamic split tension. Both pulled out and ruptured PVA fibres can be observed, where most PVA fibres were completely or partly pulled out. A complete fibre pull-out is more favourable for improving the dissipated energy as the fibre would experience a longer pull-out process. By contrast, fibre rupture or partly fibre pull-out could not contribute to improving the energy dissipation of ECC considerably. Although the RTP fibre in Fig. 14b also experienced a pull-out behaviour during the dynamic split tension, its short length and low tensile strength limited the ability to bridge the propagating crack, which is not able to enhance the energy dissipation of ECC under dynamic loadings (especially under high strain rates). A similar finding has been reported in a previous study about the dynamic split tensile behaviour of fibre reinforced geopolymer composites [40]. As confirmed in Figs. 16a and b, most PVA fibres have experienced a pull-out behaviour along with many matrix fragments on the surfaces. By contrast, fewer matrix fragments were attached to the surface of the RTP fibre, as shown in Figs. 16c and d. Because of the low tensile strength of the RTP fibre, it may break during the pull-out process, which can further weaken the energy dissipation of ECC. On the other hand, some PVA fibres could be ruptured quickly due to the superior interfacial bonding properties, impairing the energy dissipation of ECC under dynamic split tension. By contrast, most RTP fibres were completely or partly pulled out, which can partly compensate for the energy loss caused by the ruptured PVA fibres.

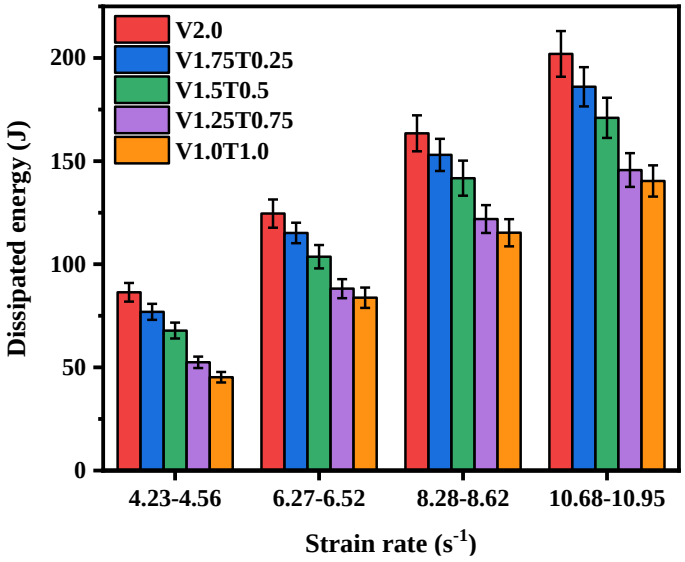

Fig. 13. Effect of RTP fibre dosage on energy dissipation of ECC under different strain rates.

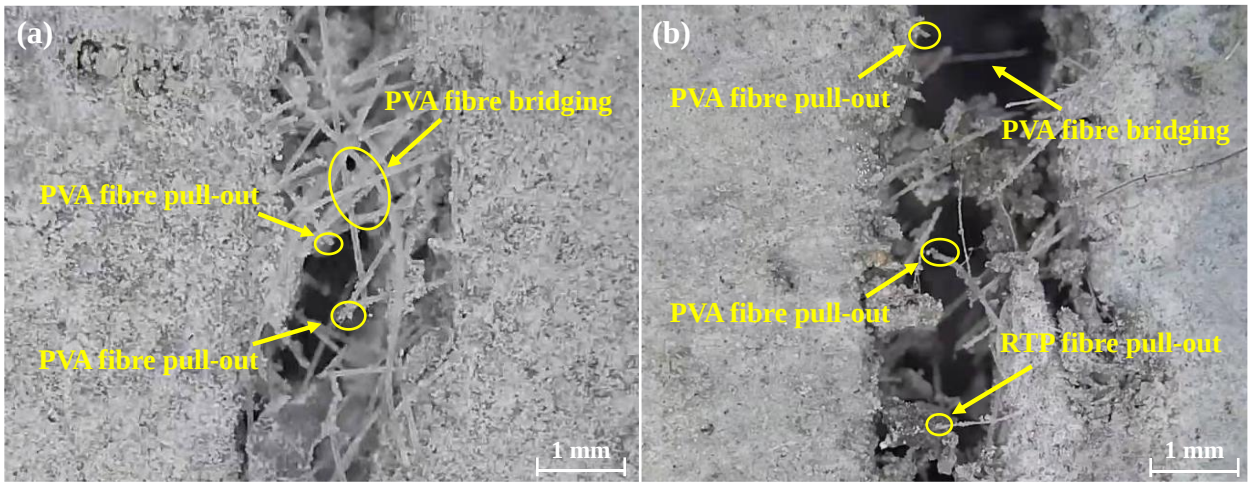

Fig. 14. Fibre conditions across the tensile fracture surfaces of ECC after dynamic split tension: (a) mono-PVA fibre reinforced ECC and (b) hybrid PVA and RTP fibre reinforced ECC.

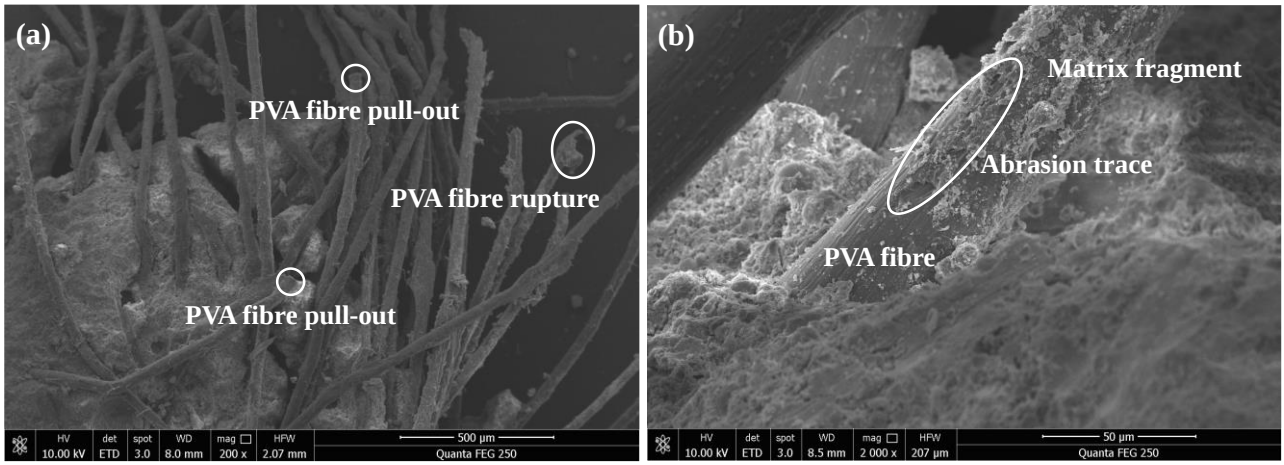

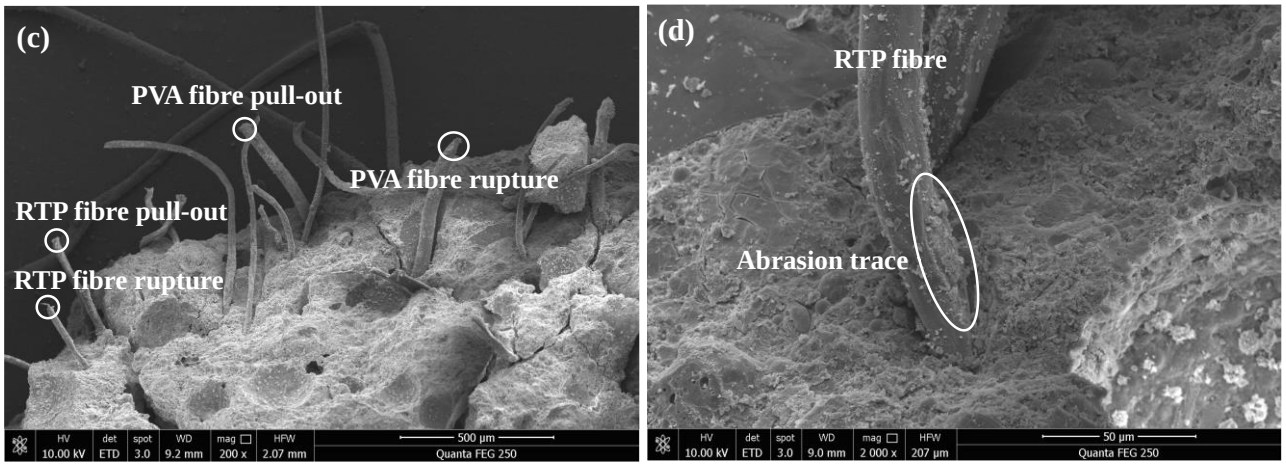

Fig. 15. SEM images of fibre morphology of ECC after dynamic split tension: (a) failure condition of PVA fibres, (b) bonding condition between PVA fibre and matrix, (c) failure condition of PVA and RTP fibres, and (d) bonding condition between RTP fibre and matrix.

3.3. Comparison between mono-PVA and hybrid PVA-RTP fibre reinforced ECC

A comprehensive comparison between mono-PVA fibre reinforced ECC and hybrid PVA-RTP fibre reinforced ECC in terms of uniaxial tensile properties, dynamic mechanical properties, and economic and environmental benefits is shown in Fig. 17, where the data of uniaxial tensile properties and dynamic compressive properties were extracted from a previous study [22]. The tensile strength (f_t) and tensile strain capacity (ε_t) were the essential parameters of ECC, which were presented in Fig. 17 to determine the optimal replacement amount of RTP fibres. When the RTP fibre content in ECC did not exceed 0.5 vol%, the static and dynamic mechanical properties of mixtures especially uniaxial tensile properties were acceptable as compared to the mix with 2.0 vol% PVA fibre. Besides, incorporating RTP fibres into ECC can significantly reduce the material cost and energy consumption of ECC, making it greener and more sustainable. Based on these results, the highest RTP replacement volume fraction should be set to 0.5%.

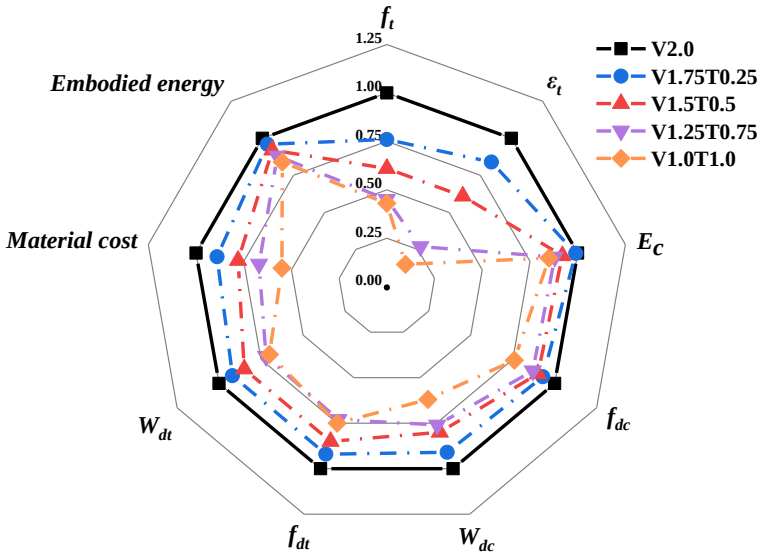

Fig. 16. A comparison between mono-PVA and hybrid PVA-RTP fibre reinforced ECC (f_t: uniaxial tensile strength, ε_t: tensile strain capacity, E_c: elastic modulus, f_{dc}: dynamic compressive strength, f_{dt}: dynamic splitting tensile strength,W_{dc}: energy absorption capacity under dynamic compression,W_{dt}: energy absorption capacity under dynamic splitting tension).

4. Conclusions

This paper systematically investigated the effect of different recycled tyre polymer (RTP) fibre replacement dosages (0.25-1.0 vol%) to polyvinyl alcohol (PVA) fibre on the split tensile behaviour of ECC under a wide range of strain rates (10^{-5} s^{-1} to 10^{1} s^{-1}). Based on the experimental results, the following conclusions can be made:

- Incorporating RTP fibres into PVA fibre reinforced ECC did not improve the uniaxial tensile behaviour and static split tensile strength of the specimen. However, ECC containing 0.5 vol% RTP fibre and 1.5 vol% PVA fibre can still show a pronounced strain-hardening and multiple cracking behaviour.
- The dynamic split tensile properties of all investigated ECC mixes including dynamic split tensile strength, dynamic increase factor (DIF) and energy dissipation were strongly sensitive to strain rate. By considering the fibre properties, a predicted logarithm equation with a R^2 of larger than 0.9 was proposed for each mixture to estimate the dynamic split tensile performance under a high strain rate.
- Similar to static mechanical properties, replacing PVA fibres with RTP fibres did not improve the dynamic split tensile properties of ECC, while the overall properties of ECC containing 0.5 vol% were still acceptable. All ECC with RTP fibres showed a stronger strain rate sensitivity as compared with the mix with PVA fibres only.

- Based on the microscopic images, most PVA fibres were completely or partly pulled out, which can greatly contribute to enhancing the dynamic split tensile strength and energy dissipation of ECC. By contrast, the poorer bonding behaviour between RTP fibres and the matrix would weaken the dynamic split tensile properties of ECC.
- A comprehensive comparison indicates that replacing PVA fibres with RTP fibres with a volume fraction of up to 0.5% was feasible to produce a greener and more economical ECC with acceptable static and dynamic mechanical properties.

References

[1] V.C. Li, Engineered Cementitious Composites (ECC): Bendable Concrete for Sustainable and Resilient Infrastructure, Springer2019.

[2] J.-X. Zhu, L.-Y. Xu, B.-T. Huang, K.-F. Weng, J.-G. Dai, Recent developments in Engineered/Strain-Hardening Cementitious Composites (ECC/SHCC) with high and ultra-high strength, Constr. Build. Mater. 342 (2022) 127956.

[3] Z. Zhang, A. Yuvaraj, J. Di, S. Qian, Matrix design of light weight, high strength, high ductility ECC, Constr. Build. Mater. 210 (2019) 188-197.

[4] J. Li, J. Qiu, J. Weng, E.-H. Yang, Micromechanics of engineered cementitious composites (ECC): A critical review and new insights, Constr. Build. Mater. 362 (2023) 129765.

[5] S. Zhou, L. Xie, Y. Jia, C. Wang, Review of cementitious composites containing polyethylene fibers as repairing materials, Polymers 12(11) (2020) 2624.

[6] J. Yu, V. Li, Research on production, performance and fibre dispersion of PVA engineering cementitious composites, Mater. Sci. Technol. 25(5) (2009) 651-656.

[7] Z. Zhang, Z. Li, J. He, X. Shi, High-strength engineered cementitious composites with nanosilica incorporated: Mechanical performance and autogenous self-healing behavior, Cem. Concr. Compos. 135 (2023) 104837.

[8] Z. Feng, Y. Zhou, L. Sui, Z. Zhu, Optimal design of a low-cost high-performance hybrid fiber engineered cementitious composites, Constr. Build. Mater. 345 (2022) 128372.

[9] M. Chen, Y. Wang, T. Zhang, M. Zhang, Microstructural evolution and dynamic compressive properties of engineered cementitious composites at elevated temperatures, J. Build. Eng. 71 (2023) 106519.

[10] X. Guan, Y. Li, T. Liu, C. Zhang, H. Li, J. Ou, An economical ultra-high ductile engineered cementitious composite with large amount of coarse river sand, Constr. Build. Mater. 201 (2019) 461-472.

[11] D. Shoji, Z. He, D. Zhang, V.C. Li, The greening of engineered cementitious composites (ECC): A review, Construction and Building Materials 327 (2022) 126701.

[12] D. Zhang, J. Yu, H. Wu, B. Jaworska, B.R. Ellis, V.C. Li, Discontinuous micro-fibers as intrinsic reinforcement for ductile Engineered Cementitious Composites (ECC), Composites, Part B 184 (2020) 107741.

[13] J.-X. Lin, Y. Song, Z.-H. Xie, Y.-C. Guo, B. Yuan, J.-J. Zeng, X. Wei, Static and dynamic mechanical behavior of engineered cementitious composites with PP and PVA fibers, Journal of Building Engineering 29 (2020) 101097.

[14] H. Zhu, K. Yu, V.C. Li, Sprayable engineered cementitious composites (ECC) using calcined clay limestone cement (LC3) and PP fiber, Cement and Concrete Composites 115 (2021) 103868.

[15] H. Zhu, D. Zhang, T. Wang, H. Wu, V.C. Li, Mechanical and self-healing behavior of low carbon engineered cementitious composites reinforced with PP-fibers, Construction and Building Materials 259 (2020) 119805.

[16] Z. Zhu, G. Tan, W. Zhang, C. Wu, Preliminary analysis of the ductility and crack-control ability of engineered cementitious composite with superfine sand and polypropylene fiber (SSPP-ECC), Materials 13(11) (2020) 2609.

[17] D. Zhang, H. Zhu, M. Hou, K.E. Kurtis, P.J. Monteiro, V.C. Li, Optimization of matrix viscosity improves polypropylene fiber dispersion and properties of engineered cementitious composites, Constr. Build. Mater. 346 (2022) 128459.

[18] H.R. Pakravan, T. Ozbakkaloglu, Synthetic fibers for cementitious composites: A critical and in-depth review of recent advances, Constr. Build. Mater. 207 (2019) 491-518.

[19] R. Merli, M. Preziosi, A. Acampora, M.C. Lucchetti, E. Petrucci, Recycled fibers in reinforced concrete: A systematic literature review, J. Clean. Prod. 248 (2020) 119207.

[20] J. Yu, J. Yao, X. Lin, H. Li, J.Y. Lam, C.K. Leung, I.M. Sham, K. Shih, Tensile performance of sustainable Strain-Hardening Cementitious Composites with hybrid PVA and recycled PET fibers, Cem. Concr. Res. 107 (2018) 110-123.

[21] H. Ehrenbring, F. Pacheco, R. Christ, B. Tutikian, Bending behavior of engineered cementitious composites (ECC) with different recycled and virgin polymer fibers, Constr. Build. Mater. 346 (2022) 128355.

[22] H. Zhong, M. Chen, M. Zhang, Engineering properties of sustainable engineered cementitious composites with recycled tyre polymer fibres, Construction and Building Materials 370 (2023) 130672.

[23] C. Lu, J. Yu, C.K.Y. Leung, Tensile performance and impact resistance of Strain Hardening Cementitious Composites (SHCC) with recycled fibers, Construction and Building Materials 171 (2018) 566-576.

[24] S.V. Samchenko, O.A. Larsen, Modifying the Sand Concrete with Recycled Tyre Polymer Fiber to Increase the Crack Resistance of Building Structures, Buildings 13(4) (2023) 897.

[25] M. Chen, H. Zhong, L. Chen, Y. Zhang, M. Zhang, Engineering properties and sustainability assessment of recycled fibre reinforced rubberised cementitious composite, J. Clean. Prod. 278 (2021) 123996.

[26] H. Zhong, M. Zhang, Effect of recycled tyre polymer fibre on engineering properties of sustainable strain hardening geopolymer composites, Cement and Concrete Composites 122 (2021) 104167.

[27] M. Serdar, A. Baričević, M. Jelčić Rukavina, M. Pezer, D. Bjegović, N. Štirmer, Shrinkage behaviour of fibre reinforced concrete with recycled tyre polymer fibres, International Journal of Polymer Science 2015 (2015).

[28] M. Chen, W. Chen, H. Zhong, D. Chi, Y. Wang, M. Zhang, Experimental study on dynamic compressive behaviour of recycled tyre polymer fibre reinforced concrete, Cem. Concr. Compos. 98 (2019) 95-112.

[29] M.J. Rukavina, A. Baricevic, M. Serdar, M. Grubor, Study on the post-fire properties of concrete with recycled tyre polymer fibres, Cem. Concr. Compos. 123 (2021) 104184.

[30] A. Baricevic, M. Pezer, M.J. Rukavina, M. Serdar, N. Stirmer, Effect of polymer fibers recycled from waste tires on properties of wet-sprayed concrete, Constr. Build. Mater. 176 (2018) 135-144.

[31] M. Chen, Z. Sun, W. Tu, X. Yan, M. Zhang, Behaviour of recycled tyre polymer fibre reinforced concrete at elevated temperatures, Cement and Concrete Composites 124 (2021) 104257.

[32] M. Chen, H. Zhong, H. Wang, M. Zhang, Behaviour of recycled tyre polymer fibre reinforced concrete under dynamic splitting tension, Cement and Concrete Composites 114 (2020) 103764.

[33] M. Chen, H. Zhong, M. Zhang, Flexural fatigue behaviour of recycled tyre polymer fibre reinforced concrete, Cement and Concrete Composites 105 (2020) 103441.

[34] L. Zhu, J. Yao, Y. Zhao, W. Ruan, G. Yang, X. Guan, Effects of composite cementation system on rheological and working performances of fresh 3D-printable engineered cementitious composites, J. Build. Eng. 65 (2023) 105801.

[35] O. Onuaguluchi, N. Banthia, Value-added reuse of scrap tire polymeric fibers in cement-based structural applications, Journal of Cleaner Production 231 (2019) 543-555.

[36] M. Chen, J. Feng, Y. Cao, T. Zhang, Synergetic effects of hybrid steel and recycled tyre polymer fibres on workability, mechanical strengths and toughness of concrete, Constr. Build. Mater. 368 (2023) 130421.

[37] D. Chen, F. Liu, F. Yang, L. Jing, W. Feng, J. Lv, Q. Luo, Dynamic compressive and splitting tensile response of unsaturated polyester polymer concrete material at different curing ages, Construction and Building Materials 177 (2018) 477-498.

[38] X. Chen, L. Ge, J. Zhou, S. Wu, Dynamic Brazilian test of concrete using split Hopkinson pressure bar, Mater. Struct. 50 (2017) 1-15.

[39] M. Chen, Y. Wang, T. Zhang, M. Zhang, Behaviour of structural engineered cementitious composites under dynamic tensile loading and elevated temperatures, Eng. Struct. 280 (2023) 115739.

[40] H. Zhong, M. Zhang, Dynamic splitting tensile behaviour of engineered geopolymer composites with hybrid polyvinyl alcohol and recycled tyre polymer fibres, Journal of Cleaner Production 379 (2022) 134779.

[41] D. Lai, C. Demartino, Y. Xiao, High-strain rate tension behavior of Fiber-Reinforced Rubberized Concrete, Cement and Concrete Composites 131 (2022) 104554.

[42] P. Pei, F. Dai, Y. Liu, M. Wei, Dynamic tensile behavior of rocks under static pre-tension using the flattened Brazilian disc method, Int. J. Rock Mech. Min. Sci. 126 (2020) 104208.

[43] Q.Z. Wang, X.M. Jia, S. Kou, Z. Zhang, P.-A. Lindqvist, The flattened Brazilian disc specimen used for testing elastic modulus, tensile strength and fracture toughness of brittle rocks: analytical

and numerical results, Int. J. Rock Mech. Min. Sci. 41(2) (2004) 245-253.

[44] C.N.L.C.M. Lewandowski Cm, Split Hopkinson (Kolsky) Bar: Design. Springer, US: Testing and Applications2015.

[45] M.I. Khan, G. Fares, S. Mourad, W.J.J.o.M.i.C.E. Abbass, Optimized Fresh and Hardened Properties of Strain-Hardening Cementitious Composites: Effect of Sand Size and Workability, Journal of Materials in Civil Engineering 28(12) (2016) 04016152.

[46] H. Zhong, Static and Dynamic Mechanical Properties of Sustainable Engineered Geopolymer Composites, UCL (University College London), 2023.

[47] G. Yang, J. Bi, Z. Dong, Y. Li, Y. Liu, Experimental Study on Dynamic Tensile Properties of Macro-Polypropylene Fiber Reinforced Cementitious Composites, Int. J. Concr. Struct. Mater. 16(1) (2022) 1-12.

[48] M.Z.N. Khan, Y. Hao, H. Hao, F.u.A. Shaikh, Mechanical properties and behaviour of high-strength plain and hybrid-fiber reinforced geopolymer composites under dynamic splitting tension, Cement and Concrete Composites 104 (2019) 103343.

[49] X. Li, Y. Zhang, C. Shi, X. Chen, Experimental and numerical study on tensile strength and failure pattern of high performance steel fiber reinforced concrete under dynamic splitting tension, Construction and Building Materials 259 (2020) 119796.

[50] J. Chen, D. Xiang, Z. Wang, G. Wu, G. Wang, Dynamic tensile strength enhancement of concrete in split Hopkinson pressure bar test, J Advances in Mechanical Engineering 10(6) (2018).

[51] S. Gurusideswar, A. Shukla, K.N. Jonnalagadda, P. Nanthagopalan, Tensile strength and failure of ultra-high performance concrete (UHPC) composition over a wide range of strain rates, Construction and Building Materials 258 (2020) 119642.

[52] H. Zhong, M. Chen, M. Zhang, Effect of hybrid industrial and recycled steel fibres on static and dynamic mechanical properties of ultra-high performance concrete, Construction and Building Materials 370 (2023) 130691.

[53] X. Chen, S. Wu, J. Zhou, Quantification of dynamic tensile behavior of cement-based materials, Construction and Building Materials 51 (2014) 15-23.

[54] H. Zhong, M. Zhang, Effect of recycled polymer fibre on dynamic compressive behaviour of engineered geopolymer composites, Ceramics International 48(16) (2022) 1151-1168.

[55] P.H. Bischoff, S.H. Perry, Compressive behaviour of concrete at high strain rates, Materials and Structures 24(6) (1991) 425-450.

[56] Y. Guo, G. Gao, L. Jing, V. Shim, Dynamic properties of mortar in high-strength concrete, Int. J. Impact Eng. 165 (2022) 104216.

[57] D. Nie, X. An, Optimization of SCC mix at paste level by using numerical method based on a paste rheological threshold theory, Constr. Build. Mater. 102 (2016) 428-434.

[58] L. Feng, X. Chen, J. Zhang, C. Chen, Experimental and mesoscopic investigation of self-compacting rubberized concrete under dynamic splitting tension, J. Build. Eng. 57 (2022) 104942.

[59] X. Zhao, Q. Li, S. Xu, Contribution of steel fiber on the dynamic tensile properties of hybrid fiber ultra high toughness cementitious composites using Brazilian test, Construction and Building Materials 246 (2020) 118416.